Improvement in Motion Efficiency of the Spirochete *Brachyspira pilosicoli* in Viscous Environments

S. Nakamura,* Y. Adachi,* T. Goto,† and Y. Magariyama‡
*School of Agriculture, Ibaraki University, Ami, Japan; †Department of Mechanical Engineering, Tottori University, Tottori, Japan; and †National Food Research Institute, Tsukuba, Japan

ABSTRACT Spirochetes are unique among swimming bacteria in terms of their lack of external flagella. They actively move in viscous environments, and, surprisingly, the swimming speed of the spirochete *Leptospira interrogans* has been reported to increase with viscosity in methylcellulose solutions. Many researchers consider that the presence of a loose, quasi-rigid network formed by linear polymer molecules is related to this strange phenomenon. One of the authors has proposed a theory that expresses this idea mathematically and successfully explains the speed properties of an externally flagellated bacterium in viscous environments. This theory predicts that the ratio of swimming speed to wave frequency (*v/f* ratio, motion efficiency in a sense) increases with viscosity. In this study, we demonstrated a new method of measuring the swimming speed and wave frequency of spirochetes and the motion characteristics of a swine intestinal spirochete, *Brachyspira pilosicoli* strain NK1f, measured in viscous environments. Several sets of swimming speed and wave frequency data were simultaneously derived from an animation obtained by our method. The *v/f* ratio of NK1f displayed a tendency to increase with increasing viscosity, suggesting the validity of the above-mentioned theory. Improvement of motion efficiency is at least one of the factors that maintain spirochete motility in viscous environments.

INTRODUCTION

Spirochetes are a group of motile bacteria with distinct morphology (1). Most are helically shaped (2), but some species have a flat sinusoidal or meandering waveform (3,4). They swim by propagating helical or flat sinusoidal waves. Their flagella do not project outward from their cell bodies, but are contained in their periplasm, which is the space between the protoplasmic cell cylinder and the outer membrane sheath (1). Each periplasmic flagellum is attached subterminally to one end of the cell cylinder and extends toward the opposite end. We know that the periplasmic flagella are the spirochetes' organelles of motility, because mutations inhibiting the synthesis of periplasmic flagella have resulted in nonmotility (5–10). Protruding periplasmic flagella, which have been observed in wild-type cells during the stationary phase and in cell cylinder helicity mutants during the exponential phase, have been shown to rotate (3,11).

Spirochetes can swim in highly viscous environments (3,12–15). Surprisingly, the swimming speed of *Leptospira interrogans* monotonically increases with viscosity up to 300 mPa × s in methylcellulose solutions (12). Externally flagellated bacteria do not have this property (16–18). For example, the swimming speed of *Pseudomonas aeruginosa* (single polar flagellation) increases with viscosity up to a characteristic point and thereafter decreases in polyvinylpyrrolidone (PVP) solutions (17). Something in the motility mechanism of spirochetes must give them this surprising ability. This attribute seems to be suitable for survival in the niches occupied by spirochetes, such as biofilm and mucus. For example, *Brachyspira pilosicoli* cells are known to attach to the apical portions of superficial enterocytes (19), suggesting that the spirochete can move in intestinal mucus covering the enterocytes.

Most of those viscous environments contain linear polymers: extracellular polysaccharides in biofilms (20), mucins in mucus (21), root mucilages in rhizosphere (22), and so on. Berg and Turner indicated in 1979 that this phenomenon was attributable to the presence of a loose, quasi-rigid network formed by linear-polymer molecules such as PVP and methylcellulose (23). Accordingly, to slow the motion of microorganisms, many researchers have used a highly branched polymer, Ficoll, which is not considered to form a network. One of the authors has successfully expressed the idea of Berg and Turner mathematically to explain the motion of externally flagellated bacteria such as *P. aeruginosa* in viscous environments (24) (Fig. 2, *a* and *b*). We can avoid the difficulty in dealing with non-Newtonian fluid to analyze the bacterial motion in polymer solutions by adopting the extremely simple assumptions in this mathematical model (Fig. 2 *a*). The above-mentioned phenomenon of the swimming speed of *P. aeruginosa* in PVP solutions is explained by this model (Fig. 3 *g*). In addition, it predicts that the ratio of swimming speed to flagellar rotation rate (*v/f* ratio) increases with viscosity (Fig. 3 *i*). The *v/f* ratio is motion efficiency in a sense because the ratio expresses the distance swum during one flagellar rotation.

Since this property of polymer solutions must be common to spirochetes and externally flagellated bacteria, we expected that this model could also be applied to spirochete motion,

Submitted September 12, 2005, and accepted for publication December 29, 2005.

Address reprint requests to Yukio Magariyama, Tel.: 81-29-838-8054; Fax: 81-29-838-7181; E-mail: maga@affrc.go.jp.

0006-3495/06/04/3019/08 $2.00

doi: 10.1529/biophysj.105.074336

with small modifications. To examine this expectation experimentally, we simultaneously measured the swimming speed and the wave frequency of *B. pilosicoli* strain NK1f isolated from swine intestine (25) by two-directional-illuminated dark-field microscopy (2DDM), which was originally developed in this study. Wave frequency of spirochetes corresponds to flagellar rotation rate of externally flagellated bacteria. The *v*/*f* ratio of NK1f increased with viscosity. In addition, we made a new model of spirochete motion in a polymer network. The model explained the experimental results.

MATERIALS AND METHODS

Spirochete strain and growth

A swine intestinal spirochete isolated in Japan, *B. pilosicoli* strain NK1f (25), was used. Cells were grown with BBL GasPac System (Becton, Dickinson, St. Louis, MO) under anaerobic conditions at 37°C for 4 days on BBL Trypticase Soy Agar (Becton, Dickinson) supplemented with 4% sheep blood. Cells scratched from the agar plate were suspended in the motility media described below. We attempted to cultivate strain NK1f in liquid medium to generate a more homogeneous cell population. The attempt was unsuccessful because, although the cell grew, harvesting them by centrifugation caused them to clump and lose much of their motility.

Preparation and viscosity measurement of motility media

The basic motility medium contained 1.5% DIFCO Casitone (Becton, Dickinson), 0.25% K2HPO4, 0.5% NaCl, 0.01 M glucose, and 400 μg/ml spectinomycin (Dainippon Pharmaceutical, Osaka, Japan). Spectinomycin was added to inhibit the growth of other bacteria because *B. pilosicoli* is resistant to the antibiotic. Each motility medium was prepared by adding polymer to 100 ml basic motility medium. PVP K90 (Wako Pure Chemical Industries, Osaka, Japan) and Ficoll Type 400 (Sigma-Aldrich, St. Louis, MO) were used as linear and highly branched polymers, respectively. Motility media were named according to the polymer species and weight, as follows: N for no polymer, P2 for 2 g PVP, F15 for 15 g Ficoll, and so on. The viscosities of the motility media were estimated from the sedimentation rates of latex beads (MX-1000; Soken Chemical and Engineering, Tokyo, Japan; 10 μm in diameter, cross-linked acrylic). When a bead falls at a constant speed v, the drag force is balanced by gravity, as

$$6\pi\mu a v = 4/3\pi a^3(\rho_B - \rho)g. \quad (1)$$

Here, μ, a, ρ_B, ρ, and g are the viscosity of the medium, radius of the bead, density of the bead, density of the medium, and gravitational acceleration, respectively. Therefore, we obtained the viscosities of the motility media as values relative to the viscosity of water, as

$$\mu = \mu_0\left(\frac{v_0}{v}\right)\frac{\rho_B - \rho}{\rho_B - \rho_0}. \quad (2)$$

Here, μ_0, v_0, v, ρ_B, ρ, and ρ_0 are the viscosity of water (0.89 mPa × s), speed of fall in water, speed of fall in the motility medium, density of the bead (1.1498 g/ml), density of the medium, and density of water. The densities of the media were measured with hydrometers. The viscosities were as follows: 0.86 mPa × s for N, 7.91 mPa × s for P2, 21.4 mPa × s for P4, 50.4 mPa × s for P6, 117 mPa × s for P8, 203 mPa × s for P10, 1.99 mPa × s for F5, 3.89 mPa × s for F10, 7.98 mPa × s for F15, 13.8 mPa × s for F20, 20.7 mPa × s for F25, and 25.8 mPa × s for F30.

2DDM apparatus

An optical filter with four divisions (Fig. 1 *b*) was constructed of two interference filters transmitting light with wavelengths of 525–575 and 625–675 nm (Koshin Kogaku, Kanagawa, Japan). This filter was set up in front of the condenser of a dark-field microscope (BX50, U-DCW, UPlanFl 40×; Olympus, Tokyo, Japan). The 2DDM images were recorded on DVCAM tapes (PDVM-40ME; Sony, Tokyo, Japan) with a DVCAM recorder (DSR-30; Sony, Tokyo, Japan) through an adaptor (U-TV1×, U-CMAD-2; Olympus) and a CCD color camera (WAT-221S; Watec, Yamagata, Japan).

Image processing and analysis

The necessary parts of the images recorded on the DVCAM tapes were captured on a PC (Endeavor Pro1100; Epson Direct, Nagano, Japan) with a video editing system (DVStorm-RT; Canopus, Hyogo, Japan). Then the swimming speed and wave frequency of each cell were determined by using Adobe Premiere, ImageJ (National Institutes of Health, Bethesda, MD) and Microsoft Excel. To minimize the effect of slow flow of the motility medium on the bacterial motion, we estimated the flow by the average motion of at least 10 latex beads (Polybead Polystyrene Microspheres 9003-53-9; Polysciences, Warrington, PA; 0.2 μm in diameter), and subtracted the flow speed from each swimming speed measured by the above method. We developed several plug-ins of ImageJ and macros of Excel to execute these processes efficiently.

RESULTS

Development of two-directional-illuminated dark-field microscopy

We developed 2DDM by applying the principle of laser dark-field microscopy (LDM (26)) to simultaneous measurement of the swimming speed and wave frequency of spirochete cells. LDM operates on the principle that the brightness change of the image of a slender body illuminated by one-directional light depends on the angle between the slender body and the light. Therefore, the image of a helical or flat sinusoidal body such as a bacterial flagellar filament is a series of bright spots, and the bright spots move along the helical axis as the wave moves. The change in brightness at a fixed position, i.e., the brightness of light passing through a slit, allows us to determine the wave frequency. In practice, LDM has been applied to simultaneous measurement of the swimming speed and flagellar rotation rate of *Vibrio alginolyticus* (27,28) and *Salmonella enterica* serovar Typhimurium (29). However, the position of the center of the helical body, which is necessary to derive the spirochete swimming speed, cannot easily be determined from the image, since the image of each spirochete cell body is broken into pieces. To solve this problem, we devised the use of two perpendicular lights of different colors (green and red in our case) in place of one-directional light in LDM. This device allowed us to objectively determine the center of the image (green and red) obtained by this illumination method, because the image of one cell is in a body and we can fit an ellipse to the image (Fig. 1 *a*). The brightness of each color changes periodically along the length of the image. The green (and red) spots move along the length as the cell wave

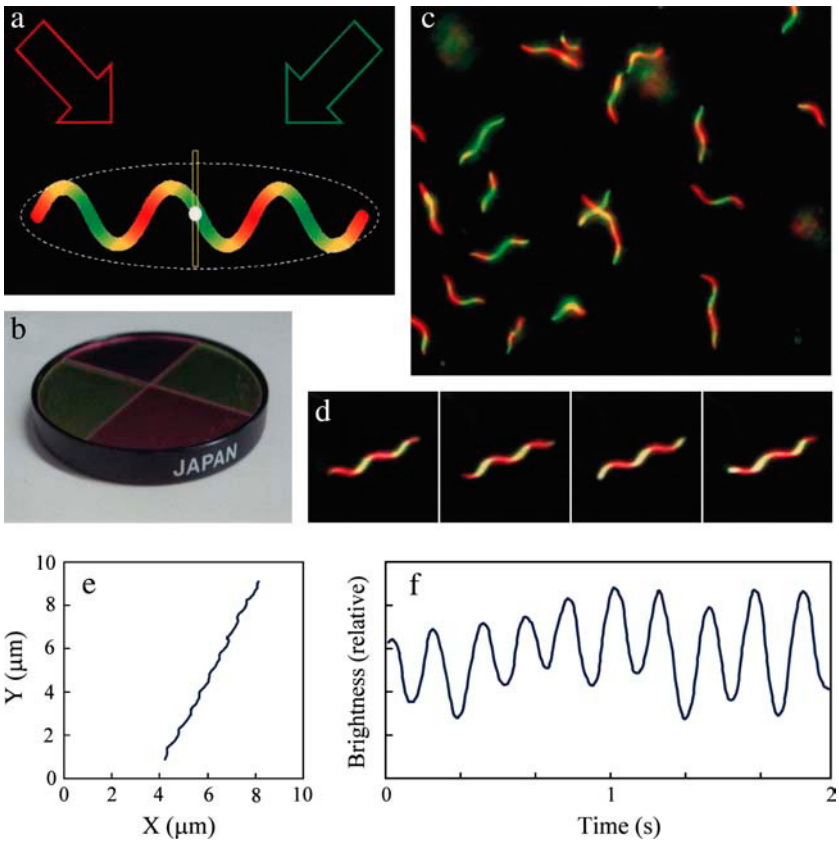

FIGURE 1 Principle of 2DDM. (*a*) Schematic drawing of the principle of 2DDM. Red and green light simultaneously illuminates a wave body from the upper left and upper right, respectively. The broken line is an ellipse fitted to the wave body and the yellow rectangle is a virtual slit. (*b*) Optical filter with four divisions. (*c*) 2DDM image of NK1f. (*d*) Sequence of 2DDM images of a swimming NK1f cell. The intervals between images were 1/30 s. (*e*) Swimming trajectory obtained by 2DDM. (*f*) Change in the green brightness at the virtual slit.

moves. Therefore, the wave frequency was determined from a monochromatic image (green) extracted from the two-color image by digital image processing.

To make a 2DDM apparatus, we set up an optical filter that consisted of four alternately arranged parts allowing the transmission of green (wavelength 525–575 nm) or red (625–675 nm) light (Fig. 1 *b*) in front of the condenser of a dark-field microscope. This filter produced the two-directional dark-field illumination. Images of NK1f obtained with this apparatus were colored green and red, as expected (Fig. 1 *c*). We obtained sequence 2DDM images (e.g., Fig. 1 *d*) by video recording. Analysis of these sequence images produced swimming trajectories and changes in green brightness at the center of each cell with time (Fig. 1, *e* and *f*). Swimming speed and wave frequency were easily determined from such data. In addition, 2DDM has an advantage in that several sets of data on swimming speed and wave frequency can simultaneously be derived from an animation because we can provide virtual slits for all the cells, in contrast to only one set by LDM.

Simultaneous measurement of swimming speed and wave frequency

B. pilosicoli strain NK1f was used in this study because its swimming speed was suitable for 2DDM measurement. Fig. 3, *a–c*, show the measured results of the motion of NK1f in polymer solutions. It is difficult to give an exact definition of the viscosity of linear-polymer solutions because such solutions are not Newtonian. We therefore estimated viscosity values from the sedimentation rates of latex beads with a diameter of 10 μm. This size is comparable to the cell length and is much larger than the cell width. We used N, P2, P4, P6, P8, P10, F5, F10, F15, F20, F25, and F30 as motility media. Note that *N* is no polymer; *P* is PVP; and *F* is Ficoll. Numbers refer to concentrations (see Materials and Methods). The swimming speeds and wave frequencies of at least 100 cells were measured for each solution. The motility data varied widely for each solution but showed an approximately normal distribution. The swimming speed in PVP solutions remained almost constant regardless of viscosity (*solid diamonds* in Fig. 3 *a*) and that in Ficoll solutions decreased with viscosity (*open diamonds* in Fig. 3 *a*). Wave frequency in both PVP and Ficoll solutions decreased with viscosity (Fig. 3 *b*). The *v*/*f* ratio in PVP solutions increased with viscosity (*solid diamonds* in Fig. 3 *c*) and that in Ficoll solutions remained almost constant (*open diamonds* in Fig. 3 *c*).

Theoretical model of spirochete motion

For comparison with our experimental results, we calculated spirochete motion by using as a framework the modified

resistive force theory proposed by Magariyama and Kudo in 2002 (24). It was difficult to calculate motion of the spirochete accurately because of the bacterium's complex structure (Fig. 2 *c*). We adopted simple assumptions to determine the equations of motion for spirochetes, as follows:

1. *Motion model of spirochete*. A helical flagellum is attached to one end of the cell body and grows inside the cell (Fig. 2 *d*). The flagellum is rotated by a flagellar motor embedded in the cell membrane. The cell body rotates in the opposite direction to the flagellar rotation because of the dynamic balance. The shape of the cell body follows that of the flagellum. No force is necessary for transformation of the cell body. The actual spirochete cell seems to completely wrap the typical externally flagellated bacterial cell in the outer membrane sheath (Fig. 2 *c*). The above-mentioned assumptions are equivalent to the rotation of the outer sheath synchronously with the rotation of the protoplasmic cylinder, and to wave propagation in the cell helix synchronously with rotation of the periplasmic flagella.
2. *Modified resistive force theory*. In resistive force theory (RFT), the hydrodynamic force and torque acting on the whole helix are obtained by integrating the force acting on a small element of the helix (28,30–33). In the modified RFT (24), we assumed that a motion can be divided into motion independent of the polymer network and motion affecting the network (see Fig. 2 *a*). The macroscopic viscosity of water (μ_0) was used as an apparent viscosity for the former and that of the polymer solution (μ) was used for the latter. In the traditional RFT, the viscosity (μ) is used for all the motions.

The balances in forces and torques are expressed under these assumptions as

$$\begin{cases} F_h = 0 \\ T_h + T_m = 0 \\ T_r - T_m = 0 \end{cases}. \tag{3}$$

Here, F_h and T_h are the drag force and torque against the helical wave change of cell body, T_r is the drag torque against the rotation of cell body, and T_m is the torque generated by the flagellar motor.

These are linear functions of swimming speed v, wave frequency ω_h, and rotation rate of cell body ω_r,

$$\begin{cases} F_h = \alpha_h v + \gamma_h \omega_h \\ T_h = \gamma_h v + \beta_h \omega_h \\ T_r = \beta_r \omega_r \\ T_m = T_0(1 - (\omega_h - \omega_r)/\omega_0) \end{cases}. \tag{4}$$

Here, T_0 and ω_0 are parameters characterizing the motor torque. α_h, β_h, γ_h, and β_r are drag coefficients. These coefficients are functions of the parameters of the spirochete shape and two apparent viscosities (μ_0 and μ) as

$$\begin{cases} \alpha_h = -C_0(8\pi^2 r^2 \mu + p^2 \mu_0) \\ \beta_h = -C_0(2r^2 p^2 \mu + 4\pi^2 r^4 \mu_0) \\ \gamma_h = C_0(4\pi r^2 p\,\mu - 2\pi r^2 p\,\mu_0) \\ \beta_r = -\frac{16}{3}\pi \mu_0 a^2 L \end{cases} \tag{5}$$

$$C_0 = \frac{2\pi L}{(\log[2p/a] - 1/2)(4\pi^2 r^2 + p^2)}.$$

Here, r, p, $2a$, and L are radius and pitch of the cell helix, and width and length of the cell body. Coefficients α_h, β_h, and γ_h are the same as those in Magariyama and Kudo (24). Coefficient β_r is for the rotation around the axis of a long cylinder.

Simultaneous Eqs. 3 and 4 can be solved analytically as

$$\begin{cases} v = K_0 \gamma_h \beta_r \\ \omega_h = -K_0 \alpha_h \beta_r \\ \omega_r = K_0(\alpha_h \beta_h - \gamma_h^2) \end{cases} \tag{6}$$

$$K_0 = \frac{T_0 \omega_0}{T_0(\alpha_h \beta_h + \alpha_h \beta_r - \gamma_h^2) - \omega_0(\alpha_h \beta_h \beta_r - \beta_r \gamma_h^2)}.$$

Therefore, the motion efficiency (*v/f* ratio) is independent of the motor torque (T_0, ω_0),

$$v/\omega_h = -\gamma_h/\alpha_h. \tag{7}$$

Fig. 3, *d–f*, shows the results calculated using the values in Table 1. The values of the shape parameters correspond to *L. interrogans* and the values of the motor characteristics correspond to *Escherichia coli* (34). The calculated swimming speed monotonically increased with viscosity (*solid line* in Fig. 3 *d*). The wave frequency calculated for spirochetes did not decrease with viscosity as much as that calculated for externally flagellated bacteria (*solid line* in Fig. 3 *e*). The *v/f* ratio also increased monotonically with viscosity (*solid line* in Fig. 3 *f*). The calculated values of swimming speed, wave frequency, and *v/f* ratio significantly differed from the measured values. This discrepancy was probably caused by the fact that the values of parameters used for the calculation were different from those of NK1f cells and the model of bacterial motion was oversimplified. We consider that the actual line for each parameter exists between the solid and broken lines in Fig. 3, *d–f*, because any actual motion is affected by the polymer network. In other words, a value between the water viscosity μ_0 and the polymer-solution viscosity μ should be adopted as the apparent viscosity for the motion parallel to the axis (see Fig. 2 *a*). However, we have no way to determine the value at present.

The results shown in Fig. 3, *a* and *b*, may have included considerable errors because the swimming speed tended to decrease gradually during the time when measurements were being taken, and many nonmotile cells ware observed. We consider that those phenomena are caused by changes in the physiological condition of the NK1f cells. On the other hand,

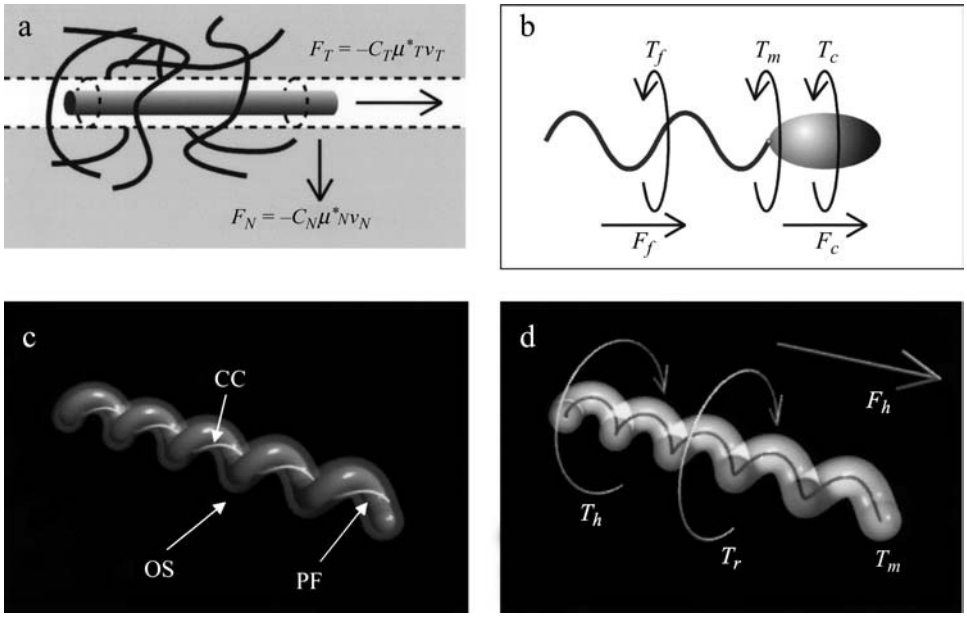

FIGURE 2 Motion models of externally flagellated bacterium and spirochete in polymer solutions. (*a*) Schematic drawing expressing the concept of modified RFT. This theory assumes that the motion can be divided into two motions: one is independent of the polymer network and the other interferes with the polymer network. The two motions are referred by apparent viscosities, μ^*_{T} and μ^*_{N}. We adopted the water viscosity, μ_0, and the macroscopic viscosity of the polymer solution, μ, as the apparent viscosities, μ^*_{T} and μ^*_{N}, in this article. (*b*) Schematic drawing of a motion model of a bacterium with a single polar flagellum. F_{c} and T_{c} are drag force and torque against the cell body, F_{f} and T_{f} is drag force and torque against the flagellar filament, and T_{m} is motor torque. Panels *a* and *b* are cited from Magariyama and Kudo (24). (*c*) Schematic drawing of spirochete structure. CC, PF, and OS indicate protoplasmic cell cylinder, periplasmic flagellum, and outer membrane sheath, respectively. (*d*) Schematic drawing of a simple model of spirochete motion. F_{h} and T_{h} are drag force and torque against helical wave change, respectively, T_{r} is drag torque against the cell-body rotation, and T_{m} is motor torque.

we consider that the *v/f* ratio was independent of the motor torque (see Eq. 7). Therefore, we conclude that the *v/f* ratio in PVP solutions was generally greater than that in Ficoll solutions of the same viscosity. This difference was clear above a viscosity of 20 mPa × s.

DISCUSSION

We demonstrated that the *v/f* ratio of NK1f cells increased with viscosity in PVP solutions. In other words, the efficiency of motion improved in viscous environments. Therefore, we conclude that improvement of motion efficiency is at least one of the factors that cause spirochetes to move actively in viscous environments.

Difference between spirochetes and externally flagellated bacteria

We consider that the unique morphology of spirochetes gives them an advantage over externally flagellated bacteria in terms of motion in viscous environments. The decrease in wave frequency of spirochetes with viscosity (Fig. 3 *e*) is probably smaller than that of externally flagellated bacteria (Fig. 3 *h*). We can theoretically explain this expectation by our model.

Equations 6 and 7 can be rearranged as functions of the solution viscosity μ as

$$\begin{cases} v = \dfrac{c_1^{\mathrm{v}}\mu + c_0^{\mathrm{v}}}{d_1^{\mathrm{v}}\mu + d_0^{\mathrm{v}}} \\ \omega_{\mathrm{h}} = \dfrac{c_1^{\omega}\mu + c_0^{\omega}}{d_1^{\omega}\mu + d_0^{\omega}} \\ \dfrac{v}{\omega_{\mathrm{h}}} = \dfrac{c_1^{\mathrm{e}}\mu + c_0^{\mathrm{e}}}{d_1^{\mathrm{e}}\mu + d_0^{\mathrm{e}}} \end{cases}. \tag{8}$$

Here, $c_{\mathrm{i}}^{\mathrm{x}}$ and $d_{\mathrm{i}}^{\mathrm{x}}$ are coefficients. Since $(\alpha_{\mathrm{h}}\beta_{\mathrm{h}} - \gamma_{\mathrm{h}}^2)$ has no second-order term of μ, the denominators of the swimming speed and wave frequency are first-order of μ. Equation 8 indicates that the swimming speed, wave frequency, and *v/f* ratio approach nonzero values as viscosity approaches infinity.

In the case of a single polar flagellated bacterium, the above equations change into the following equations (24):

$$\begin{cases} F_{\mathrm{c}} + F_{\mathrm{f}} = 0 \\ T_{\mathrm{f}} + T_{\mathrm{m}} = 0 \\ T_{\mathrm{c}} - T_{\mathrm{m}} = 0 \end{cases}, \tag{9}$$

$$\begin{cases} F_{\mathrm{c}} = \alpha_{\mathrm{c}} v \\ T_{\mathrm{c}} = \beta_{\mathrm{c}}\omega_{\mathrm{c}} \\ F_{\mathrm{f}} = \alpha_{\mathrm{f}} v + \gamma_{\mathrm{f}}\omega_{\mathrm{f}} \\ T_{\mathrm{f}} = \gamma_{\mathrm{f}} v + \beta_{\mathrm{f}}\omega_{\mathrm{f}} \\ T_{\mathrm{m}} = T_0(1 - (\omega_{\mathrm{f}} - \omega_{\mathrm{c}})/\omega_0) \end{cases}, \tag{10}$$

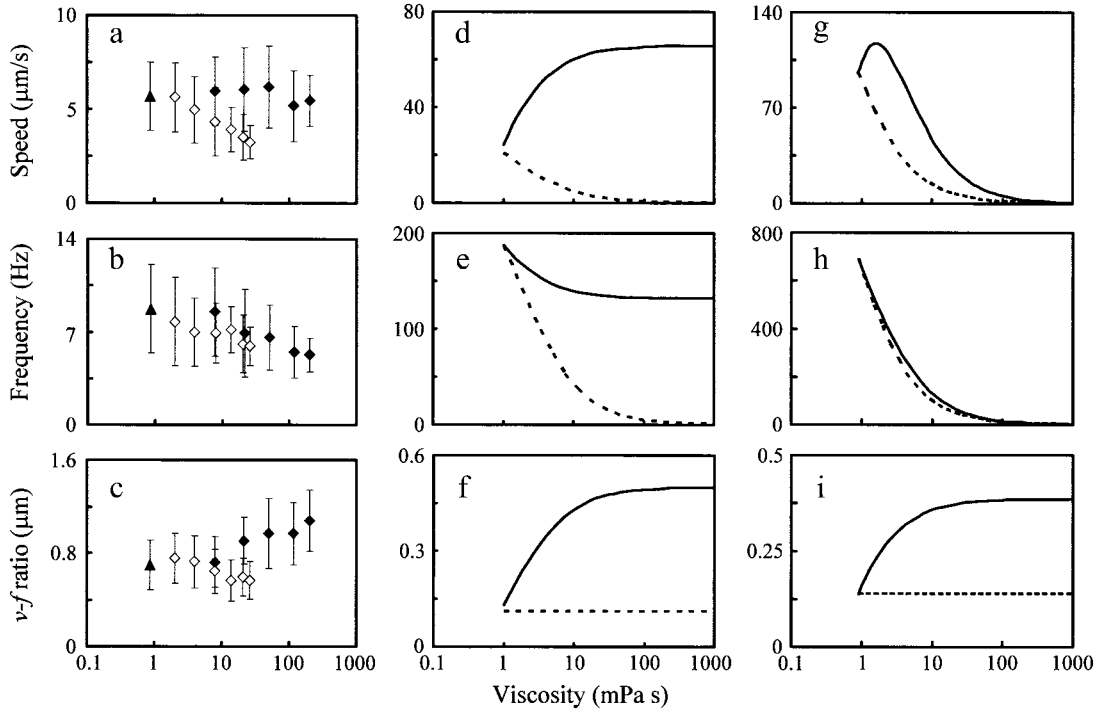

FIGURE 3 Parameters of motion in viscous environments obtained by the experiment and the calculation. (*a–c*) Results of NK1f measured by 2DDM. The symbols ▲, ♦, and ◇ refer to data from no-polymer, PVP, and Ficoll solutions, respectively. Symbols refer to means and bars to standard deviations of at least 100 measurements. (*d–f*) Results calculated for spirochete using Eq. 6 and values in Table 1. (*g–i*) Results calculated for externally flagellated bacterium using Eq. 12 and values in Table 1. Solid and broken lines refer to results obtained using modified and traditional RFTs, i.e., for linear and highly branched polymer (PVP and Ficoll) solutions, respectively. (*a*, *d*, *g*) Swimming speed. (*b*, *e*, *h*) Wave frequency or flagellar rotation rate. (*c*, *f*, *i*) *v*/*f* ratio.

$$\begin{cases} \alpha_c = -6\pi\mu a\left\{1-\frac{1}{5}\left(1-\frac{b}{a}\right)\right\} \\ \beta_c = -8\pi\mu_0 a^3\left\{1-\frac{3}{5}\left(1-\frac{b}{a}\right)\right\} \\ \alpha_f = -C_0(8\pi^2 r^2\mu + p^2\mu_0) \\ \beta_f = -C_0(2r^2p^2\mu + 4\pi^2 r^4\mu_0) \\ \gamma_f = C_0(4\pi r^2 p\,\mu - 2\pi r^2 p\,\mu_0) \\ C_0 = \dfrac{2\pi L}{(\log[2p/d]-1/2)(4\pi^2 r^2 + p^2)} \end{cases}, \quad (11)$$

$$\begin{cases} v = K_0\beta_c\gamma_f \\ \omega_f = -K_0(\alpha_c\beta_c + \alpha_f\beta_c) \\ \omega_c = K_0(\alpha_c\beta_f + \alpha_f\beta_f - \gamma_f^2) \\ K_0 = T_0\omega_0/\{T_0(\alpha_c\beta_c + \alpha_c\beta_f + \alpha_f\beta_c + \alpha_f\beta_f - \gamma_f^2) \\ \qquad -\omega_0(\alpha_c\beta_c\beta_f + \alpha_f\beta_c\beta_f - \beta_c\gamma_f^2)\} \end{cases}, \quad (12)$$

$$v/\omega_f = -\gamma_f/(\alpha_c + \alpha_f), \quad (13)$$

$$\begin{cases} v = \dfrac{c_1^v\mu + c_0^v}{d_2^v\mu^2 + d_1^v\mu + d_0^v} \\ \omega_f = \dfrac{c_1^\omega\mu + c_0^\omega}{d_2^\omega\mu^2 + d_1^\omega\mu + d_0^\omega} \\ \dfrac{v}{\omega_f} = \dfrac{c_1^e\mu + c_0^e}{d_1^e\mu + d_0^e} \end{cases}. \quad (14)$$

In contrast to the calculation for spirochetes, the denominators of the swimming speed and wave frequency have μ^2-terms. Therefore, the swimming speed and flagellar rotation rate of externally flagellated bacteria approach zero as viscosity approaches infinity.

As viscosity approaches infinity, the flagellar rotation rate of an externally flagellated bacterium approaches zero (Fig. 3 *h*), but the wave frequency of a spirochete approaches a finite value (Fig. 3 *e*) according to the theoretical analyses. Our measured wave frequency did not contradict this prediction (Fig. 3 *b*). However, this property of spirochetes is not self-evident. The mechanisms by which spirochetes move must give them this advantage. We plan to examine the effect of the spirochete shape on these three parameters of motility, swimming speed, wave frequency, and *v*/*f* ratio.

Unknown ability of spirochetes?

Modified RFT, which considers the structure of polymer solution, can explain most of the motility properties of spirochetes in polymer solutions. However, the wave frequency decreased with viscosity as gradually in Ficoll solutions as in PVP solutions (Fig. 3 *b*), a result not predicted by the RFT calculation. That is, the wave frequency in the Ficoll solutions (*open diamonds* in Fig. 3 *b*) did not agree with the calculated ones (*dashed line* in Fig. 3 *e*). The decrease in swimming speed with viscosity was also not as great (*open diamonds* in Fig. 3 *a*). However, the *v*/*f* ratio measured in the Ficoll solutions was almost constant (Fig. 3 *c*). These results suggest that in addition to the structure of polymer solution, active control of motility by the spirochete itself is involved in this phenomenon.

TABLE 1 Parameters necessary for calculating bacterial motion

Parameter	Symbol	Value
For spirochete		
Radius of cell helix	r	0.05 μm
Pitch of cell helix	p	0.5 μm
Width of cell body	$2a$	0.1 μm
Length of cell body	L	10 μm
Motor torque at rotation rate of 0	T_0	0.5×10^{-18} N $\times$ m
Rotation rate at motor torque of 0	ω_0	300 rps
For externally flagellated bacterium		
Cell width	$2b$	0.80 μm
Cell length	$2a$	1.92 μm
Diameter of flagellar filament	$2d$	0.032 μm
Length of flagellar filament	L	5.02 μm
Pitch of flagellar helix	p	1.58 μm
Radius of flagellar helix	r	0.14 μm
Motor torque at rotation rate of 0	T_0	1.5×10^{-18} N $\times$ m
Rotation rate at motor torque of 0	ω_0	1700 rps
Viscosity of water	μ_0	0.89 mPa $\times$ s

The values for externally flagellated bacterium were cited from Magariyama and Kudo (24).

It is possible that motor power increases with increased viscous drag in spirochetes. Some marine *Vibrio* species are known to express lateral flagella in response to decreased rates of rotation of the polar flagellum, e.g., caused by increased viscosity (35–37), and some peritrichously flagellated bacteria form more flagella on surfaces or viscous media (38). It will be interesting to see whether spirochetes respond to increasing viscosity by increasing motor output.

The deformation of spirochete shape is another possibility. Hydrodynamic forces cause elastic deformation of the spirochete cell. Parameters of motion such as swimming speed and wave frequency must be affected if the elastic deformation is significant. In addition, the hydrodynamic force may cause discrete deformation, i.e., polymorphism. For externally flagellated bacteria, the elastic flagellar deformation and the polymorphic transitions caused by fluid force have been studied by high-intensity dark-field microscopy: elongation of *Salmonella* close-coiled flagellar filaments (39), normal-to-curly transition for *S. enterica* serovar Typhimurium (40), and normal-to-coil transition for *Rhodobacter sphaeroides* (41). However, precise changes in the shape of swimming spirochetes have not yet been measured. That information may reveal alterations of length, width, wave form, and pitch number of swimming cells that are important components for efficient swimming.

SUPPLEMENTARY MATERIAL

An online supplement to this article can be found by visiting BJ Online at http://www.biophysj.org.

We thank K. Namba and S. Sugiyama for their comments on the manuscript, and K. Nakazawa for measurement of viscosity.

This work was supported in part by grants from the Yamada Science Foundation and Sekisui Chemical.

REFERENCES

1. Charon, N. W., and S. F. Goldstein. 2002. Genetics of motility and chemotaxis of a fascinating group of bacteria: the spirochetes. *Annu. Rev. Genet.* 36:47–73.
2. Holt, S. C. 1978. Anatomy and chemistry of spirochetes. *Microbiol. Rev.* 42:114–160.
3. Goldstein, S. F., N. W. Charon, and J. A. Kreiling. 1994. *Borrelia burgdorferi* swims with a planar waveform similar to that of eukaryotic flagella. *Proc. Natl. Acad. Sci. USA.* 91:3433–3437.
4. Goldstein, S. F., K. F. Buttle, and N. W. Charon. 1996. Structural analysis of *Leptospiraceae* and *Borrelia burgdorferi* by high-voltage electron microscopy. *J. Bacteriol.* 178:6539–6545.
5. Charon, N. W., E. P. Greenberg, M. B. H. Koopman, and R. J. Limberger. 1992. Spirochete chemotaxis, motility, and the structure of the spirochetal periplasmic flagella. *Res. Microbiol.* 143:597–603.
6. Li, C., J. Ruby, N. Charon, and H. Kuramitsu. 1996. Gene inactivation in the oral spirochete *Treponema denticola*: construction of a *flgE* mutant. *J. Bacteriol.* 178:3664–3667.
7. Limberger, R. J., L. L. Slivienski, J. Izard, and W. A. Samsonoff. 1999. Insertional inactivation of *Treponema denticola tapI* results in a non-motile mutant with elongated flagellar hooks. *J. Bacteriol.* 181:3743–3750.
8. Li, C., M. A. Motaleb, M. Sal, S. F. Goldstein, and N. W. Charon. 2000. Spirochete periplasmic flagella and motility. *J. Mol. Microbiol. Biotechnol.* 2:345–354.
9. Motaleb, M. A., L. Corum, J. L. Bono, A. F. Elias, P. Rosa, D. S. Samuels, and N. W. Charon. 2000. *Borrelia burgdorferi* periplasmic flagella have both skeletal and motility functions. *Proc. Natl. Acad. Sci. USA.* 97:10899–10904.
10. Picardeau, M., A. Brenot, and I. Saint Girons. 2001. First evidence for gene replacement in *Leptospira* spp. Inactivation of *L. biflexa flaB* results in non-motile mutants deficient in endoflagella. *Mol. Microbiol.* 40:189–199.
11. Charon, N. W., S. F. Goldstein, S. M. Block, K. Curci, J. D. Ruby, J. A. Kreiling, and R. J. Limberger. 1992. Morphology and dynamics of protruding spirochete periplasmic flagella. *J. Bacteriol.* 174:832–840.
12. Kaiser, G. E., and R. N. Doetsch. 1975. Enhanced translational motion of *Leptospira* in viscous environments. *Nature.* 255:656–657.
13. Greenberg, E. P., and E. Canale-Parola. 1977. Relationship between cell coiling and motility of spirochetes in viscous environments. *J. Bacteriol.* 131:960–969.
14. Kimsey, M. J., and A. Spielman. 1990. Motility of Lyme disease spirochetes in fluids as viscous as the extracellular matrix. *J. Infect. Dis.* 162:1205–1208.
15. Ruby, J. D., and N. W. Charon. 1998. Effect of temperature and viscosity on the motility of the spirochete *Treponema denticola*. *FEMS Microbiol. Lett.* 169:251–254.
16. Shoesmith, J. G. 1960. The measurement of bacterial motility. *J. Gen. Microbiol.* 22:528–535.
17. Schneider, W. R., and R. N. Doetsch. 1974. Effect of viscosity on bacterial motility. *J. Bacteriol.* 117:696–701.
18. Strength, W. J., B. Isani, D. M. Linn, F. D. Williams, G. E. Vandermolen, B. E. Laughon, and N. R. Krieg. 1976. Isolation and characterization of *Aquaspirillum fasciculus* sp. Nov., a rod-shaped, nitrogen-fixing bacterium having unusual flagella. *Int. J. Sys. Bacteriol.* 26:253–268.
19. Trott, D. J., C. R. Huxtable, and D. J. Hamson. 1996. Experimental infection of newly weaned pigs with human and porcine strains of *Serpulina pilosicoli*. *Infect. Immun.* 64:4648–4654.
20. Christensen, B. E. 1989. The role of extracellular polysaccharides in biofilms. *J. Bacteriol.* 10:181–182.

21. Mantle, M., G. Stewart, G. Zayas, and M. King. 1990. The disulphide-bond content and rheological properties of intestinal mucins from normal subjects and patients with cystic fibrosis. *Biochem. J.* 266:597–604.

22. Traore, O., V. Groleau-Renaud, S. Plantureux, A. Tubeileh, and V. Boeuf-Tremblay. 2000. Effect of root mucilage and modeled root exudates on soil structure. *Eur. J. Soil Sci.* 51:575–581.

23. Berg, H. C., and L. Turner. 1979. Movement of microorganisms in viscous environments. *Nature.* 278:349–351.

24. Magariyama, Y., and S. Kudo. 2002. A mathematical explanation of an increase in bacterial swimming speed with viscosity in linear-polymer solutions. *Biophys. J.* 83:733–739.

25. Tasu, C., T. Tanaka, T. Tanaka, and Y. Adachi. 2004. *Brachyspira pilosicoli* isolated from pigs in Japan. *J. Vet. Med. Sci.* 66:875–877.

26. Kudo, S., Y. Magariyama, and S.-I. Aizawa. 1990. Abrupt changes in flagellar rotation observed by laser dark-field microscopy. *Nature.* 346:677–680.

27. Magariyama, Y., S. Sugiyama, K. Muramoto, Y. Maekawa, I. Kawagishi, Y. Imae, and S. Kudo. 1994. Very fast flagellar rotation. *Nature.* 371:752.

28. Magariyama, Y., S. Sugiyama, K. Muramoto, I. Kawagishi, Y. Imae, and S. Kudo. 1995. Simultaneous measurement of bacterial flagellar rotation and swimming speed. *Biophys. J.* 69:2154–2162.

29. Magariyama, Y., S. Sugiyama, and S. Kudo. 2001. Bacterial swimming speed and rotation rate of bundled flagella. *FEMS Microbiol. Lett.* 199:125–129.

30. Hancock, G. J. 1953. The self-propulsion of microscopic organisms through liquids. *Proc. R. Soc. Lond. A.* 217:96–121.

31. Gray, J., and G. J. Hancock. 1955. The propulsion of sea-urchin spermatozoa. *J. Exp. Biol.* 32:802–814.

32. Holwill, M. E. J., and R. E. Burge. 1963. A hydrodynamic study of the motility of flagellated bacteria. *Arch. Biochem. Biophys.* 101:249–260.

33. Chwang, A. T., and T. Y. Wu. 1971. A note on the helical movement of micro-organisms. *Proc. R. Soc. Lond. B Biol. Sci.* 178:327–346.

34. Berg, H. C. 2003. The rotary motor of bacterial flagella. *Annu. Rev. Biochem.* 72:19–54.

35. Kawagishi, I., M. Imagawa, Y. Imae, L. McCarter, and M. Homma. 1996. The sodium-driven polar flagellar motor of marine *Vibrio* as the mechanosensor that regulates lateral flagellar expression. *Mol. Microbiol.* 20:693–699.

36. Atsumi, T., Y. Maekawa, T. Yamada, I. Kawagishi, Y. Imae, and M. Homma. 1996. Effect of viscosity on swimming by the lateral and polar flagella of *Vibrio alginolyticus*. *J. Bacteriol.* 178:5024–5026.

37. McCarter, L. L. 2001. Polar flagellar motility of the *Vibrionaceae*. *Microbiol. Mol. Biol. Rev.* 65:445–462.

38. McCarter, L. L. 2004. Dual flagellar systems enable motility under different circumstances. *J. Mol. Microbiol. Biotechnol.* 7:18–29.

39. Hoshikawa, H., and R. Kamiya. 1985. Elastic properties of bacterial flagellar filaments. *Biophys. Chem.* 22:159–166.

40. Macnab, R. M., and M. K. Ornston. 1977. Normal-to-curly flagellar transition and their role in bacterial tumbling. Stabilization of an alternative quaternary structure by mechanical force. *J. Mol. Biol.* 112:1–30.

41. Armitage, J. P., and R. M. Macnab. 1987. Unidirectional, intermittent rotation of flagellum of *Rhodobacter sphaeroides*. *J. Bacteriol.* 169: 514–518.